Mengyu Li
College of Mechanical and Electrical Engineering,
Harbin Engineering University,
Harbin, Heilongjiang 150001, China
e-mail: 812647328@qq.com

Christopher C. Bernitsas
Marine Renewable Energy Laboratory,
Department of Naval Architecture & Marine Engineering,
University of Michigan,
2600 Draper Road,
Ann Arbor, MI 48109-2145;
Intern; Detroit Country Day—Upper School,
22305 West, 13 Mile Road,
Beverly Hills, MI 48025
e-mail: bernitsasch@northvilleschools.net

Jing Guo
Department of Mathematical Sciences,
Worcester Polytechnic Institute,
Worcester, MA 01609
e-mail: jguo3@wpi.edu

Hai Sun[1]
College of Mechanical and Electrical Engineering,
Harbin Engineering University,
Harbin, Heilongjiang 150001, China;
Marine Renewable Energy Laboratory,
Department of Naval Architecture & Marine Engineering,
University of Michigan,
2600 Draper Road,
Ann Arbor, MI 48109-2145;
Vortex Hydro Energy,
Ann Arbor, MI 48105
e-mail: sunhai2009@gmail.com

Synergistic Flow-Induced Oscillation of Multiple Cylinders in Harvesting Marine Hydrokinetic Energy

Flow-induced oscillations/vibrations (FIO/V) of cylinders in tandem can be enhanced by proper in-flow spacing to increase hydrokinetic energy harnessing. In a farm of multiple cylinders in tandem, the effect of interference on harnessing efficiency arises. Three years of systematic experiments in the Marine Renewable Laboratory (MRELab) of the University of Michigan, on an isolated cylinder, and two and three cylinders in tandem have revealed that synergistic FIO can enhance oscillations of cylinders in close proximity. Two cylinders in tandem can harness 2.5–13.5 times the hydrokinetic power of one isolated cylinder. Three cylinders in tandem can harness 3.4–26.4 times the hydrokinetic power of one isolated cylinder. Negative impact on the harnessed energy by multiple cylinders, such as the shielding effect for the downstream cylinder/s, is possible. Specifically for the three-cylinder configuration, at a certain flow speed, the decrease in the power of the middle cylinder can be overcome by adjusting its stiffness and/or damping. [DOI: 10.1115/1.4048877]

Keywords: vortex-induced vibration, galloping, tandem cylinders, synergistic enhancement, hydrokinetic energy, fluid–structure interaction, ocean energy technology

1 Introduction

Rigid cylinders on elastic supports in transverse flows can be excited in FIO, thus converting marine hydrokinetic (MHK) energy to mechanical energy in oscillators. Vortex-induced vibration (VIV) and galloping are the most commonly occurring FIO and are implemented in the vortex-induced vibrations for aquatic clean energy (VIVACE) converter mechanics [1,2]. This current energy converter (CEC) is equipped with one or more cylinders on springs, in transverse flow, which responds in FIO. Each cylinder is connected to a power take-off system. An important question in the fluid–structure interaction (FSI) mechanics of this Alternating Lift Technology (ALT) [3] converter is how interactions affect the synergy between multiple cylinders. This interaction affects directly both the numerator and the denominator of the power-to-volume density. This metric is the Achilles heel of all renewable energy technologies. Fish in schools move effortlessly by proper placement in the wake of fish ahead of them [4]. In FIO of multiple cylinders in tandem, previous studies show that the interactions, especially in the transition region from VIV to galloping, can enhance the oscillation of both cylinders [3,5]. VIVACE is being developed to achieve optimal FSI synergy among cylinders in a school so that it can operate as a real 3D converter instead of a point absorber (buoy), line absorber (Pelamis), or area absorber (oscillating water column, turbine).

Multi-cylinder tests have been conducted in the Low Turbulence Free Surface Water (LTFSW) Channel in the Marine Renewable Energy Laboratory (MRELab) at the University of Michigan [6–9] for Reynolds numbers in the range $30{,}000 \leq \mathrm{Re} \leq 120{,}000$, which falls in the high-lift TrSL3 flow regime [10]. Results show that the synergy of FSI for four cylinders can produce power as much as 80% more than four cylinders in isolation and the overall efficiency can reach 88% [7] of the Betz limit [11–13]. In this paper, selective cases of tests conducted over three years of systematic research on the harnessed power of one, two, and three cylinders in tandem are presented. Damping, spacing ratio, and stiffness are used as testing parameters. The cylinder response is measured, and the power output is calculated thereof. Turbulence simulation, in the form of roughness strips, is applied to induce galloping and, thus, increase the harnessed MHK power. This also increases the range of FSI synchronization over which VIVACE can operate efficiently. The recently developed second generation of the spring-damping controller, V_{ck}, in the MRELab enables embedded computer-controlled change of viscous damping and spring-stiffness for precise oscillator modeling and fast parameter changes for systematic testing [8]. Experimental results for harvested power by one and two cylinders and the supporting data on amplitude and frequency response are presented in Ref. [9]. The objectives of this work are as follows: (a) to study experimentally the synergy between multiple cylinders in FIO in a two and a three-cylinder VIVACE converter, and (b) to

[1]Corresponding author.

Contributed by the Ocean, Offshore, and Arctic Engineering Division of ASME for publication in the Journal of Offshore Mechanics and Arctic Engineering. Manuscript received May 18, 2020; final manuscript received October 13, 2020; published online November 18, 2020. Editor: Lance Manuel.

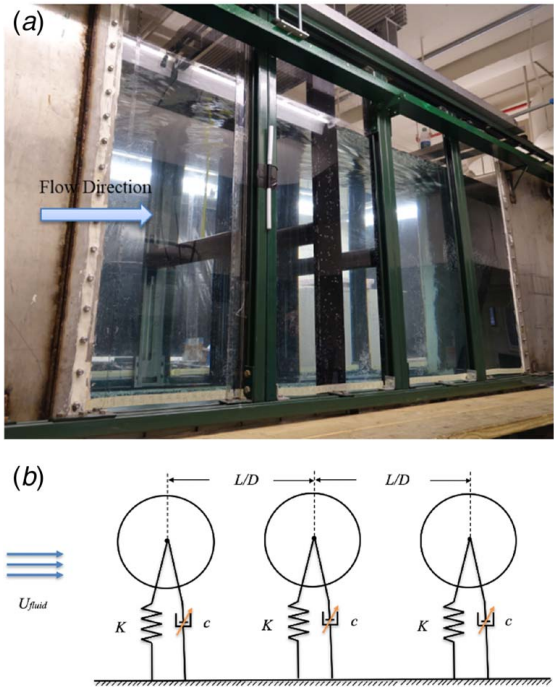

Fig. 1 Three-cylinder VIVACE converter with V_{ck}: (*a*) in the LTFSW Channel and (*b*) schematic design

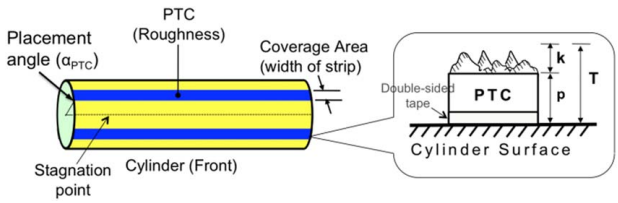

Fig. 2 Configuration of the passive turbulence control (PTC) on the cylinder [17]

evaluate the impact of the interaction of the tandem cylinder configuration on the overall power conversion performance compared to a single isolated cylinder in FIO.

2 Physical Model

The basic VIVACE converter consists of a single circular cylinder suspended on end-springs, variable mass and damping, and a power take-off (PTO) system. In this study, the physical model consists of three oscillators each with its own V_{ck} controller enabling variable spring-stiffness and damping. Each cylinder has distributed surface roughness [14,7] as passive turbulence control.

2.1 Experimental Facility: Recirculating Channel. Tests were conducted in the LTFSW Channel, in the MRELab at the University of Michigan. The channel recirculates 37,854 lt (10,000 gallons) of freshwater at a speed up to 1.5 m/s using an impeller powered by a 20-hp induction motor. The test section is 2.44 m long, 1.0 m wide, and made of transparent plexiglass, enabling visualization of flow using two 5-W argon lasers and Al_2O_3 particles of 100 μm. The water depth was set at 1.17 m and the flow speed limited to 1.35 m/s for safety from galloping. Figure 1 shows a three-oscillator system in the channel.

2.2 Cylinders and Distributed Surface Roughness. The hydrodynamic excitation applied to the cylinder is a result of FSI. To enhance cylinder flow-induced oscillations (FIO)—a form of FSI—to harness more MHK energy, distributed roughness in the form of roughness strips was introduced and extensively studied in the MRELab experimentally [12] and numerically [6]. Multiple cylinders in FIO/V are also research areas in marine engineering [15,16]. The distributed roughness was termed passive turbulence control (PTC). This study resulted in a most valuable tool, the PTC-to-FIV (fluid induced vibration) map [17,18]. As shown in Fig. 2, PTC consists of a pair of straight roughness strips attached to the surface of the cylinder symmetrically with respect to the flow direction. According to the PTC-to-FIV map (Fig. 3), the location of the roughness strips determines the FIO/V response of the cylinder. In this study, the placement angle was set at $\alpha_{PTC} =$ 20 deg, measured in degrees from the forward stagnation point to the upstream edge of the roughness strip. Based on previous studies [17,18] on PTC, sandpaper strips with commercial roughness designation P60 and width of 12.7 mm, which cover 16 deg on each side of the 88.9 mm diameter cylinder, are used in this study. Table 1 shows the details of the turbulence stimulation.

The total thickness of the PTC is on the order of the boundary layer thickness. The robustness of the PTC-to-FIV map was studied by Park et al. [18], defining not only the PTC coverage requirement in the direction of the flow but also the hierarchy of dominance of the zones where PTC is applied.

2.3 Oscillator Simulated by the V_{ck} System. For systematic experimental testing, particularly in such a large design space, two challenges are important to overcome: (a) changing the physical springs and dampers requires extensive calibration and alignment time. (b) The viscous damping of the system is rarely linear as modeled in classical vibration textbooks. To overcome these two challenges, the MERLab developed the first-generation V_{ck}

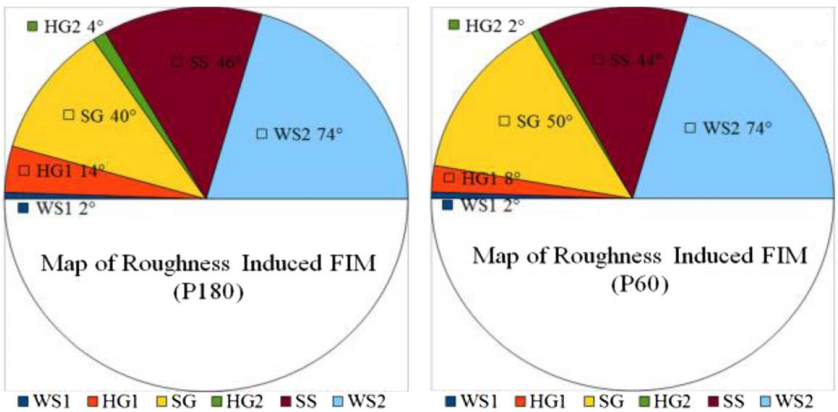

Fig. 3 The PTC-to-FIV map [18]

Table 1 PTC parameters (P60)

Strip placement angle	α_{PTC} (deg)	20
Angular coverage of strip	θ (deg)	16
Sandpaper plus tape thickness	P (mm)	0.587
Average grit height	k (mm)	0.26
The total thickness of the strip	$T = P + k$ (mm)	0.847

Table 2 Specifications of the experimental apparatus (model converter)

Mass ratio	Aspect ratio	Maximum oscillatory amplitude	Longitudinal distance
$0.634 \le m^* \le 2.00$	$L/D = 10.07$	$A_{max}/D_{3.5"} = 5.5$	$1.429 \le d/D_{3.5"} \le 6.0$

controller in 2008–2010 [19] and the second generation in 2013–2015 [8]. In both generations of V_{ck}, the controller force in the V_{ck} model is expressed as

$$F_{controller} = F_{nonlinear\_damping} - c_{virtual}\dot{y} - K_{virtual}y \tag{1}$$

where $F_{controller}$ is the force applied by the controller (Arduino Due), $F_{nonlinear\_damping}$ is the total nonlinear damping force, $K_{virtual}$ is the virtual spring constant, and $c_{virtual}$ is the virtual linear viscous damping coefficient.

Designing and implementing the V_{ck} system involves extensive system identification and comparison with physical springs and dampers. Two are the strongest advantages of the V_{ck} system: (a) the hydrodynamic force is not included in the control loop; that would have biased the measured phenomenon of VIV or galloping. (b) It should be clarified that the term virtual means that the actual force is indeed applied but forced through the controller rather than a physical spring and a physical damper. V_{ck} can readily implement any spring or damping model (linear, nonlinear, or adaptive) and any parametric for such models.

The features of the model of the oscillator are summarized in Table 2. In the current model design, the linear-motion-transmission mechanism was placed underwater, which resulted in most of the oscillator components being underwater. The whole linear-motion system, which consists of the end sliding-blocks, one timing belt, and pulleys, is fitted inside of a 38-mm wide slender tube. Figure 4 shows the side view of a single and two oscillators with the V_{ck} mounted in the LTFSW channel.

3 Mathematical Model of the Harness Power and Efficiency

3.1 Harnessed and Dissipated Power. The flow is in the x-direction. The motion of the cylinder in the y-direction is modeled by the second-order linear differential equation of an oscillator as

$$m_{osc}\ddot{y} + c_{total}\dot{y} + Ky = F_{Fluid} \tag{2}$$

where y is the direction perpendicular to the flow and the cylinder axis m_{osc} is the total oscillating system mass, which includes one-third of the spring-mass, K is the spring-stiffness, C_{total} is the total damping coefficient, and F_{Fluid} is the force exerted by the fluid on the body in the y-direction.

In order to convert hydrokinetic energy to mechanical energy in the oscillator and subsequently electrical energy, additional damping is introduced into the system. The total damping (C_{total}) is defined as

$$c_{total} = c_{structure} + c_{harness} \tag{3}$$

where $c_{stucture}$ is the existing damping due to losses in the transmission system. In this research, the value of $c_{structure}$ is adjusted by the

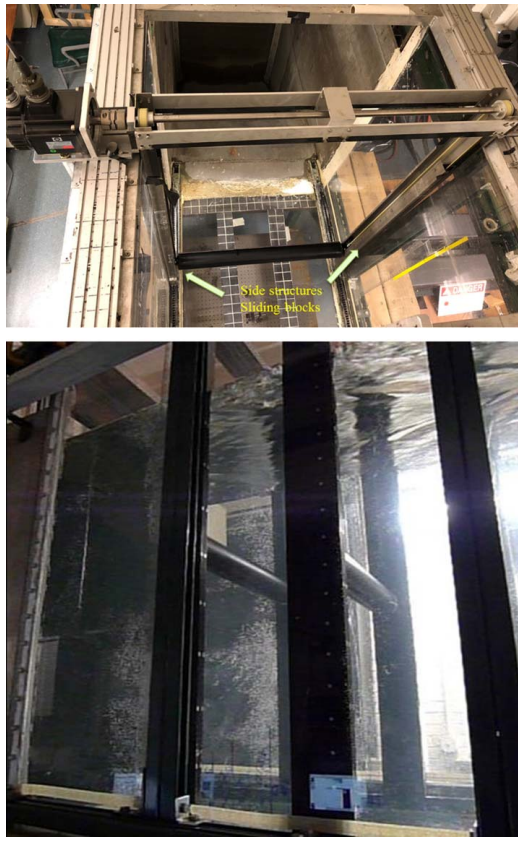

Fig. 4 Single and two-oscillator converter with V_{ck} mounted in the LTFSW channel (top and side views)

V_{ck} controller according to m^* and K in order to achieve a round $\zeta_{structure}$ that makes plotting and comparing results much easier to read and use in design. $c_{harness}$ is the damping added through V_{ck} that converts the mechanical energy in the oscillating cylinder to electrical energy for harnessing.

From Eq. (3), we know that $C_{structure}$ and $C_{harness}$ can be expressed using the damping ratio $\zeta_{harness}$ and $\zeta_{structure}$

$$\zeta_{structure} = \frac{c_{structure}}{2\sqrt{m_{osc}K}} \tag{4}$$

$$\zeta_{harness} = \frac{c_{harness}}{2\sqrt{m_{osc}K}} \tag{5}$$

Then, the mechanical power of VIVACE can be expressed as [20]

$$\begin{aligned} P_{VIVACE-Mech} &= \frac{1}{T_{osc}}\int_0^{T_{osc}} 4\pi(m_{osc}+m_a)\zeta_{total}\dot{y}^2 f_{n,water}\,dt \\ &= 8\pi^3(m_{osc}+m_a)\zeta_{total}(Af_{osc})^2 f_{n,water} \end{aligned} \tag{6}$$

Using Eq. (6), we obtain the harnessed power and the dissipated power as

$$P_{VIVACE-structure} = 8\pi^3(m_{osc}+m_a)\zeta_{structure}(Af_{osc})^2 f_{n,water} \tag{7}$$

$$P_{VIVACE-harness} = 8\pi^3(m_{osc}+m_a)\zeta_{harness}(Af_{osc})^2 f_{n,water} \tag{8}$$

Since Eqs. (7) and (8) appear to depend explicitly on the added mass m_a, it is worth noting that they can be recast using as follows [9], respectively.

$$P_{VIVACE-dissipated} = \frac{1}{2}c_{structure}A^2\omega_{osc}^2 \tag{9}$$

Table 3 Particulars of test settings

	Cylinder/s
L/D = cylinder spacing	2.01
K(N/m) = spring-stiffness	400, 600, 800, 1000
Temperature (°C)	20.5
μ (N s/m^2) = dynamic viscosity	1.004E−03
ν (m^2/s) = kinematic viscosity	9.940E−07
ρ (kg/m^3) = *water density*	999.729
D (m) = *cylinder diameter*	0.0889
L (m) = *cylinder length*	0.895
$m_{displacement}$ (kg)	5.425
m_{osc} (kg); equivalent oscillating mass not including added mass	7.286
m_{added} *(kg)*	5.425
$\zeta_{structure}$ = damping ratio	0.020
$\zeta_{harnessed}$ = damping ratio	0.16, 0.20, 0.24
$f_{n,water}$ = natural frequency in quiescent water	0.89–1.55
$f_{n,vac}$ = natural frequency in vacuum	1.18–1.86

and

$$P_{VIVACE-harness} = \frac{1}{2} c_{harness} A^2 \omega_{osc}^2 \tag{10}$$

where A is the amplitude of the cylinder oscillation and ω_{osc} is the angular frequency, which can be measured using the encoder of the motor of the V_{ck} system. These two equations do not depend on the specific way the added mass is calculated or even the value of the added mass explicitly. A detailed derivation of the above equations is provided by Ref. [9].

As a final note on this short mathematical model, it is important to mention that a controversy exists regarding the value of m_a used in Eqs. (4) and (5) and also in

$$f_{n,water} = \frac{1}{2\pi} \sqrt{\frac{K}{m_{osc} + m_a}} \tag{11}$$

There are two approaches. In the first, the added mass is included as a constant added mass from potential theory. In the second approach, the calculated added mass from the lift force in-phase with the acceleration in the y-direction is used [21]. It is the author's opinion that this controversy is unnecessary as both are simple modeling methods that cannot account for the range of synchronization or the self-limiting nature of the amplitude of oscillation. Both just model the response of the cylinder in fluid induced motion (FIM) for specific flow velocity and a given experiment. On the other hand, both approaches are useful in post-processing data and understanding this complex phenomenon better. For a better understanding of the complexity of the added mass expression in forces and moments on a small body moving with a 6D motion in a 3D unsteady flow, the reader is referred to the detailed analysis by Foulhoux and Bernitsas [22]. The dependence of the inertia terms on absolute and/or relative velocity as well as the form of convective terms is explained thoroughly putting into perspective the simplicity of the inertia term used in Morison et al.'s equation [23].

More recently though, Ref. [24] proved theoretically and confirmed experimentally the existence of an eigen relation at the interface between fluid and structure. They also derived analytical expressions for the forces and force phases in monochromatic FIO. These expressions matched with amazing accuracy all experimental observations and measurements on VIV and galloping of a solid cylinder in one degree-of-freedom transverse oscillation.

3.2 Power Conversion Efficiency. The power in a fluid is calculated based on the area swept by the cylinders [9]

$$P_{Fluid} = \frac{1}{2} \rho U^3 (2A_{\max} + D) L \tag{12}$$

where U is the flow velocity, ρ is the water density, $A_{\max}$ is the largest amplitude among all cylinders in a multiple-cylinder converter, D is the cylinder diameter, and L is the cylinder length. This expression appears in the denominator of the efficiency Eqs. (13) and (14) below. The additional complexity here is that the area swept by the cylinders depends on Amax—the cylinder response. Contrary, for propellers or wind turbines, the flow area is determined by the fixed geometry of the area swept by the blades. The Betz limit is the theoretical maximum power that can be extracted from an open flow and is equal to 59.26% (=16/27). Based on the Betz limit, the power conversion efficiency, $\eta_{convert}$, and power harness efficiency, $\eta_{harness}$, can be calculated as

$$\eta_{convert}(\%) = \frac{P_{convert}}{P_{Fluid} \times Betz\ limit} \times 100 \tag{13}$$

$$\eta_{harness}(\%) = \frac{P_{harness}}{P_{Fluid} \times Betz\ limit} \times 100 \tag{14}$$

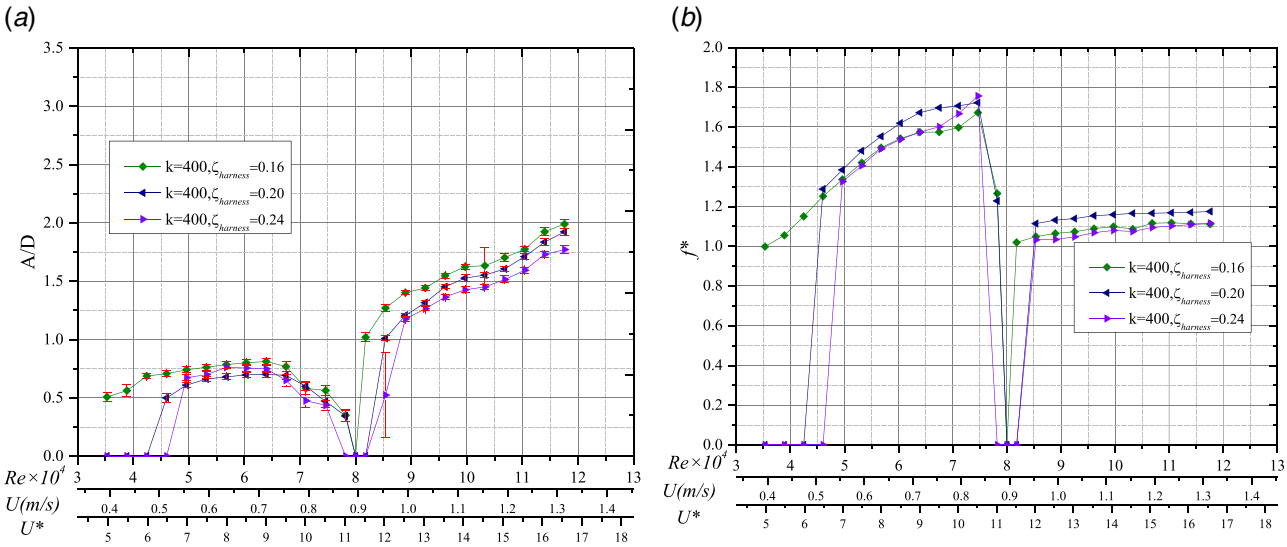

Fig. 5 Oscillatory response of single isolated cylinder at $K = 400$ N/m and $m^* = 1.343$: (*a*) amplitude ratio A/D and (*b*) frequency ratio $f^* = f_{osc}/f_{n,water}$, Ref. [5]. (Color version online.)

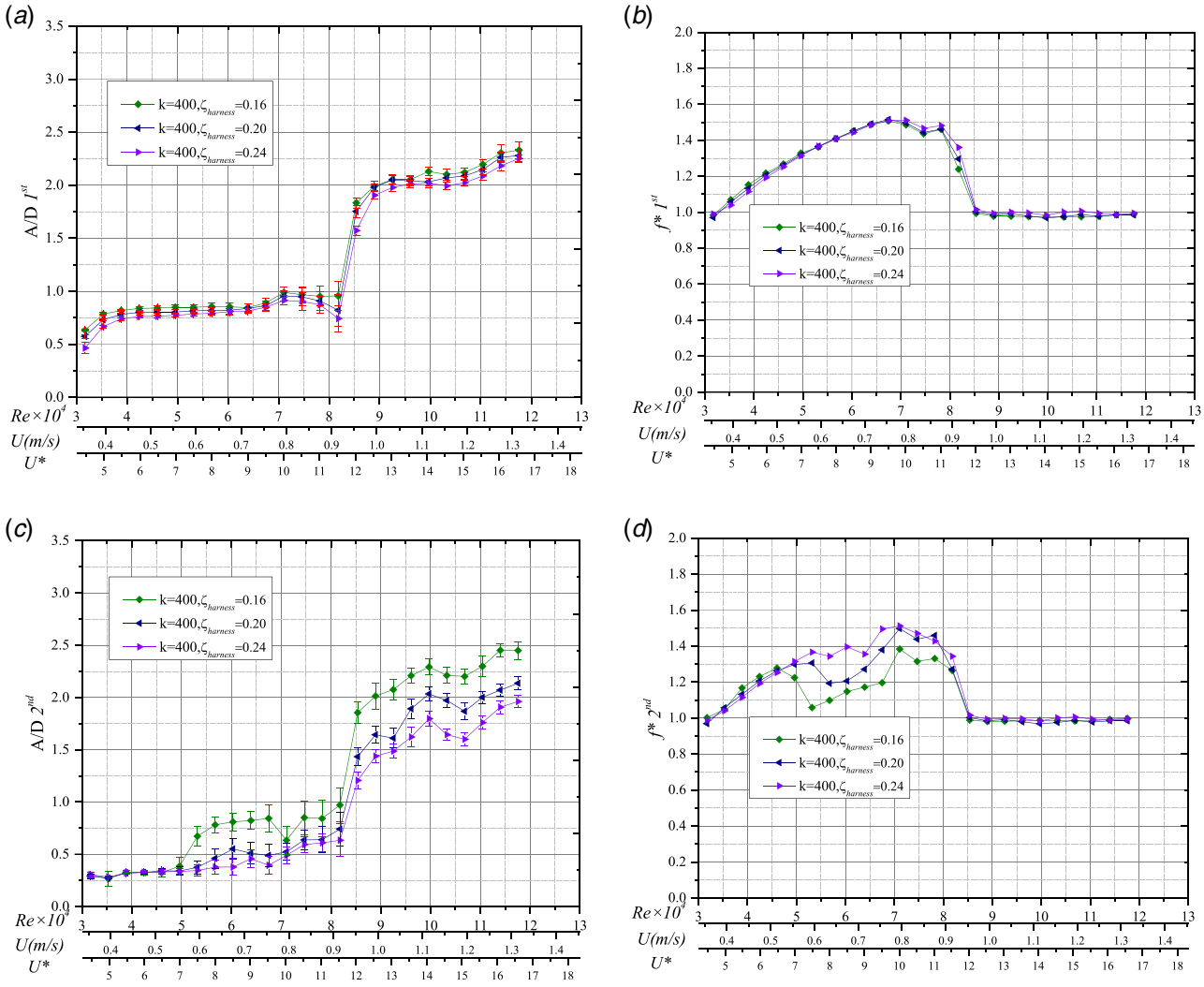

Fig. 6 Oscillatory response of two tandem cylinders at $K = 400$ N/m, $m^* = 1.343$, and $L/D = 2.01$: (*a*) *A/D* upstream, (*b*) frequency ratio *f upstream, (*c*) *A/D* downstream, and (*d*) frequency ratio *f** downstream (Color version online.)**

Commercial-scale wind turbines with three blades achieve a peak efficiency of 75–80% of the Betz limit. The VIVACE converter achieves efficiency up to 88% with four cylinders in tandem [7].

4 Results and Discussion

A series of experiments were conducted to measure the flow-induced oscillations of one, two, and three tandem cylinders with the following parametric ranges: Spring-stiffness of $K =$ 400–1000N/m; damping ratio range of $0.16 \le \zeta_{harness} \le 0.24$; longitudinal center-to-center spacing ratio $L/D = 2.01$; and mass ratio $m^* = 1.343$.

In Sec. 4.1, we provide a comparison of the oscillatory responses of one, two and three cylinder converters. Extensive results for a single cylinder were published by Ref. [8] and for two cylinders by Ref. [9]. The FIO of three-cylinder converter is presented and studied in Sec. 4.2.

The experimental parameter values are shown in Table 3. The stiffness K selected is accurate in form (linear function) and exact in parametric values as they are defined by the calibrated motor torque and its relation to the rotation in the V_{ck} controller. That is, the K value is not subjected to fabrication error or degradation in time due to fatigue. Similarly, the values of $\zeta_{harness}$ and ζ_{total} are exact, and the corresponding linear viscous function is accurate as explained in the discussion on the V_{ck} system (Sec. 2.3). The flow velocity range is 0.35 m/s $\le U \le 1.35$ m/s, Reynolds number range is $30{,}000 \le \mathrm{Re} \le 120{,}000$, and the corresponding reduced velocity range is $2.92 \le U^* \le 15.33$. All three cylinders are identical and the parameters of the corresponding oscillator are set by three independent V_{ck} systems.

4.1 Oscillatory Response Comparison of One- and Two-Cylinder Converters.

The amplitude A of a cylinder in FIO is calculated by averaging the absolute values of the 30 highest values of positive and 30 highest negative peaks in 60 s of running time past the transient. The mean absolute deviation is denoted by vertical red bars (Figs. 5–7). The frequency ratio $f^* = f_{osc}/f_{n,water}$ is plotted versus reduced velocity $U^* = U/Df_{n,water}$. The oscillation frequency f_{osc} is calculated by discrete Fourier transform (DFT) of the time history of the cylinder after the exclusion of the beginning and end transients.

The amplitude and frequency response of cylinders in FIO are divided into three ranges:

(a) $30{,}000 \le \mathrm{Re} \le 75{,}000$: Initial, upper, and lower branches of VIV.
- *Initial branch*: For an isolated cylinder (Fig. 5), the VIV onset flow velocity of the oscillation increases as the additional (harnessing) damping ratio increases. The second (Fig. 6) and third (Fig. 7) tandem cylinders oscillate for

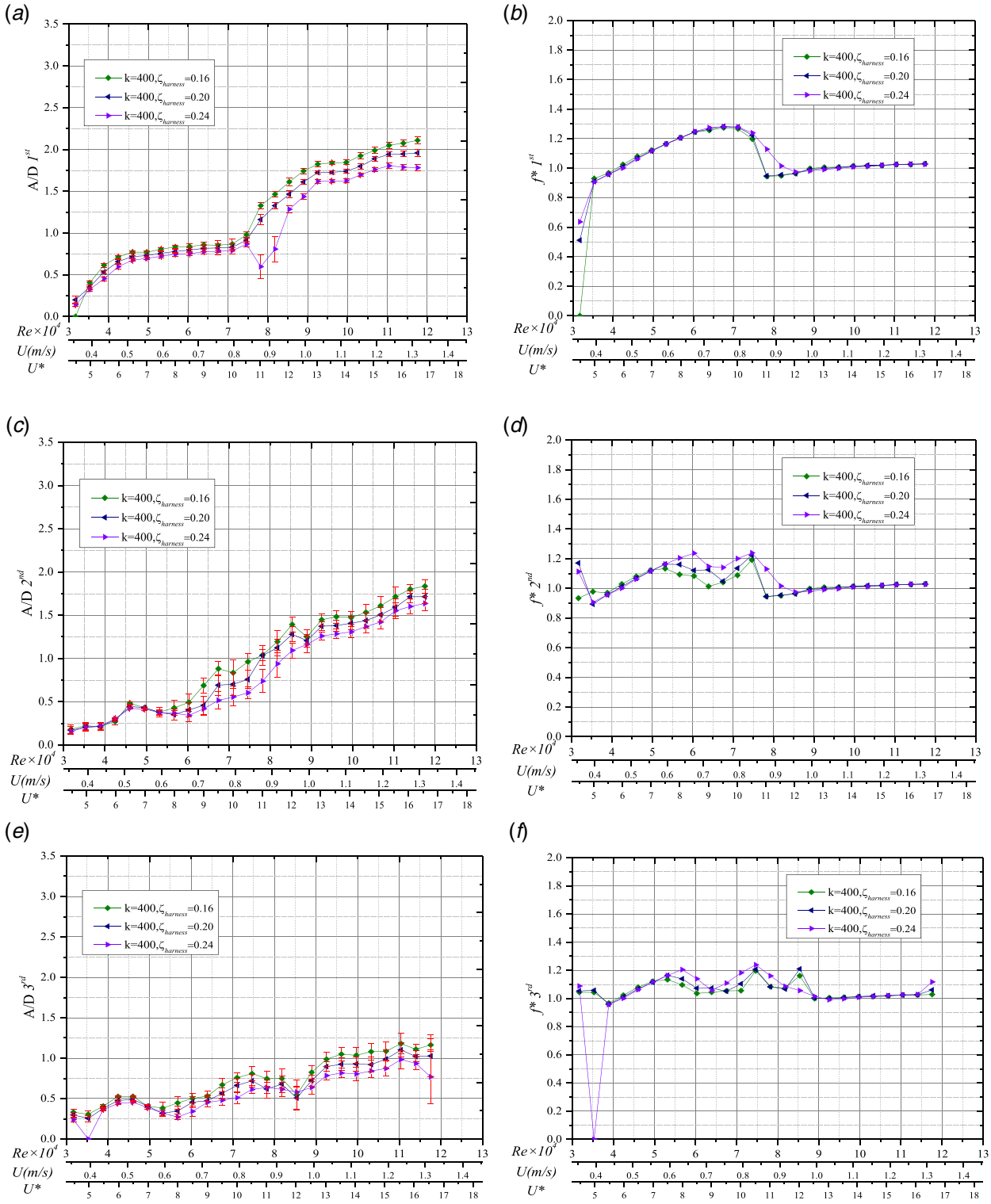

Fig. 7 Oscillatory response of three tandem cylinders at $K = 400$ N/m, $m^* = 1.343$, and $L/D = 2.01$: (a) *A/D*, first cylinder; (b) frequency ratio, first; (c) *A/D*, second cylinder; (d) frequency ratio, second cylinder; (e) *A/D*, third cylinder; and (f) frequency ratio, third cylinder (Color version online.)

all the tested damping and stiffness values. For two tandem cylinders, the downstream cylinder is half-suppressed in this region. For three tandem cylinders, however, the second and third cylinders' frequency is higher than that of the first one.

- *Upper branch*: The single isolated cylinder has a narrower upper branch, due to the relatively high damping of this study for energy harnessing ($\zeta_{harness} = 0.16$, 0.20, and 0.24) (Fig. 5(*a*)). In the multiple cylinder cases (Figs. 6(*a*), 6(*c*), 4(*a*), 4(*c*), and 4(*e*)), however, this trend is not observed. The presence of the tandem cylinders broadens the upper branch for the upstream/first cylinder. The amplitudes of the downstream cylinder/s are suppressed as the damping increases. On the other hand, the frequency increases as the damping ratio increases.

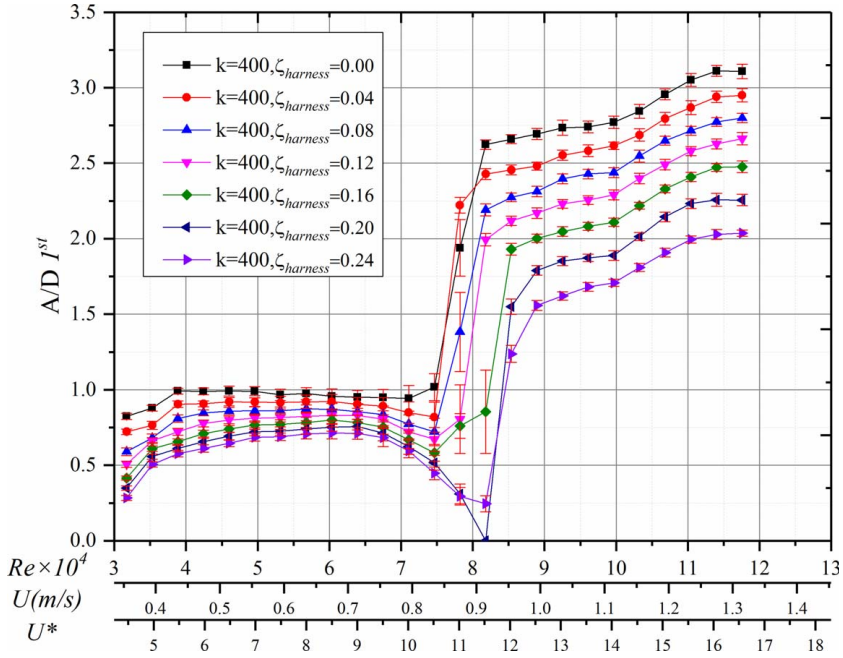

Fig. 8 The *A/D* of $K = 400$ N/m of the first cylinder at $L/D = 2.57$

- *Lower branch*: There are no obvious lower branches for the second and third cylinders (Figs. 6(*c*), 7(*c*), and 7(*e*)) as galloping initiates leaving no gap in the transition from VIV to galloping. The upstream cylinder presents this phenomenon as the damping increases. All frequencies drop in this range.

(b) $68{,}000–70{,}000 \leq \mathrm{Re} \leq 80{,}000–90{,}000$ includes the desynchronization range, the gap between VIV and galloping, and the onset of galloping.

- A gap between VIV and galloping appears in the single-cylinder cases. Oscillation ceases for higher damping values $\zeta_{harness} = 0.24$ (Fig. 18). Specifically, the gap appears because damping reduces the amplitude response in VIV and delays the onset of galloping. In the cases of multiple cylinders, however, gaps are not observed. The presence of the downstream cylinders enhances the oscillation of all cylinders in this region. Specifically, galloping initiates at the beginning of this range for the second cylinder in the three-cylinder case. The explanation for this observation is that galloping is caused by asymmetry in the relative flow, which is due to both the geometric asymmetry due to turbulence stimulation and the upstream flow asymmetry due to the wake of upstream cylinders.
- The frequency response for multiple cylinders drops to the natural frequency in water.

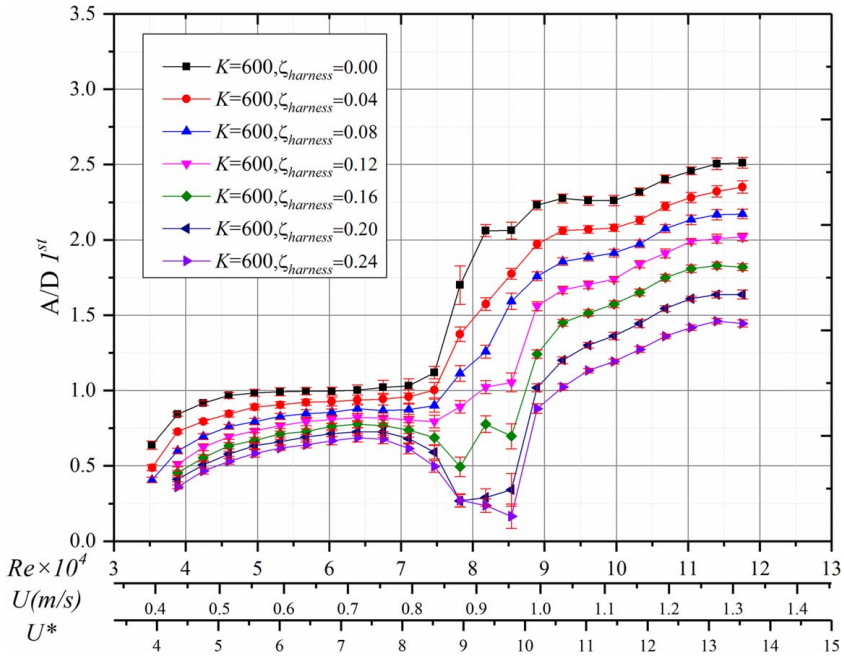

Fig. 9 The *A/D* of $K = 600$ N/m of the first cylinder at $L/D = 2.57$

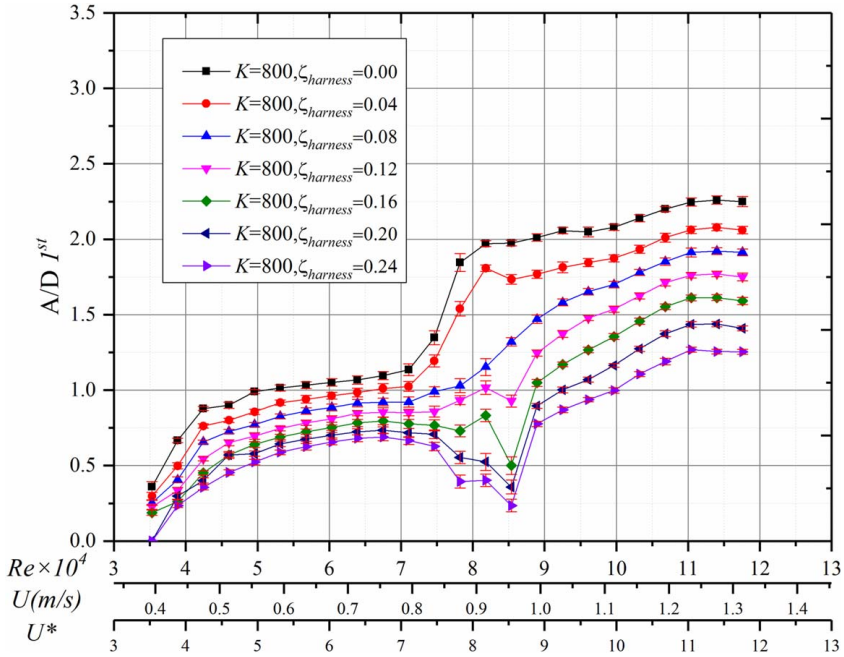

Fig. 10 The *A/D* of $K = 800$ N/m of the first cylinder at $L/D = 2.57$

(c) 80,000–90,000 ≤ Re is the galloping region.

- For the single isolated cylinder, the amplitude rises as the flow velocity increases. For the two tandem cylinders, after a certain velocity is reached, their amplitude rises quickly as the flow velocity increases. The amplitude of three tandem cylinders shares the same features with the single cylinder.
- At the last tested flow speed, the amplitude of the third cylinder starts to drop, due to visibly increased three-dimensionality in the flow and tip-flow effects (Fig. 7).
- The frequency response remains at the natural frequency in quiescent water for all cylinders, in all cases, regardless of the settings.

4.2 Oscillation Response of Three Tandem Cylinders. For the three cylinders in tandem, for spacing $L/D = 2.57$ and $m^* = 1.343$, the measured amplitude ratio is presented in Figs. 8–12 for the first cylinder, Figs. 13–16 for the second cylinder, and Figs. 17–20, for the third cylinder. Due to the second cylinder, both the upstream (first) and the downstream (second) cylinder exhibit some interesting response features as discussed below.

Flow-Induced Oscillation of the First Cylinder. The amplitude ratio measurements for the three tandem cylinders are presented in Figs. 8–11 for four different values of K and seven values of $\zeta_{harness}$. For comparison, corresponding results for the singe isolated cylinder for $K = 400$ N/m and the same range of $\zeta_{harness}$ are

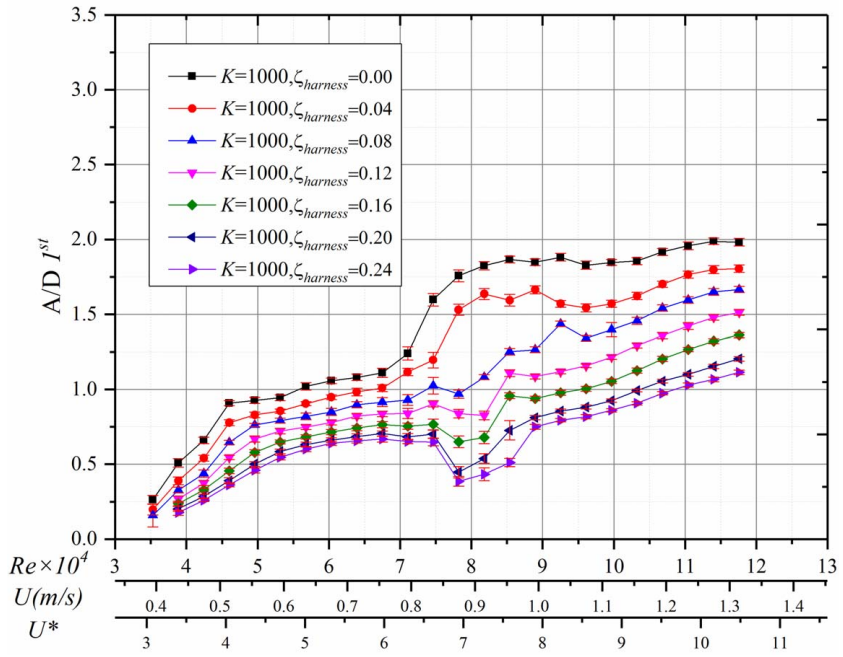

Fig. 11 The *A/D* of $K = 100$ N/m of the first cylinder at $L/D = 2.57$

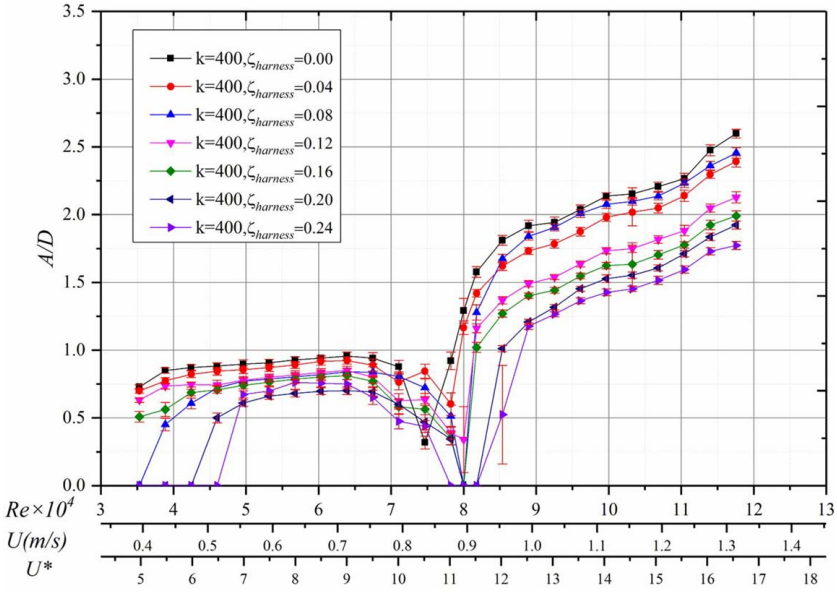

Fig. 12 Comparison of the single isolated cylinder at $K = 400$ N/m

presented in Fig. 12. The presence of the second cylinder has a significant impact on the upstream cylinder, which is consistent with previous work by Ref. [9] for two tandem cylinders.

Some distinctive differences between the single isolated cylinder and the upstream (first) cylinder in a tandem formation can be observed.

(1) The first cylinder in tandem undergoes VIV much earlier than the single, isolated cylinder. Specifically, the onset of VIV for the first cylinder in tandem occurs for Re = 31,000 for all harnessed damping ratios tested. The VIV onset for an isolated cylinder occurs at Re = 35,000 only at the lower harnessing damping ratios of 0.00–0.12. At the higher end of damping (ζharness > 0.12), the VIV onset Reynolds number increases to 38,900 (ζharness = 0.16), 45,000 (ζharness = 0.20), and 48,000 (ζharness = 0.20). The fact that the onset flow velocity changes for higher damping ratio shows that the FIO of the lower branch for the isolated cylinder is unstable. On the other hand, the upstream cylinder in tandem shows very stable FIO even at the initial VIV branch. A comparison is shown in Fig. 21. The upstream cylinder exhibits stable oscillation and higher frequency. The phase portrait shows that the upstream cylinder maintains a higher oscillation speed, which is important to have higher harnessed power (Sec. 4.1).

(2) The transition region initiates around Re = 70,000 for both the upstream cylinder and the isolated one. At lower harnessing damping ratios, the first cylinder in tandem shows stable oscillation with no sign of dropping the amplitude before galloping is reached. At higher damping, except for the highest damping tested, the cylinder still oscillates. The FIO of the isolated cylinder shows a sign of slowing down and at a

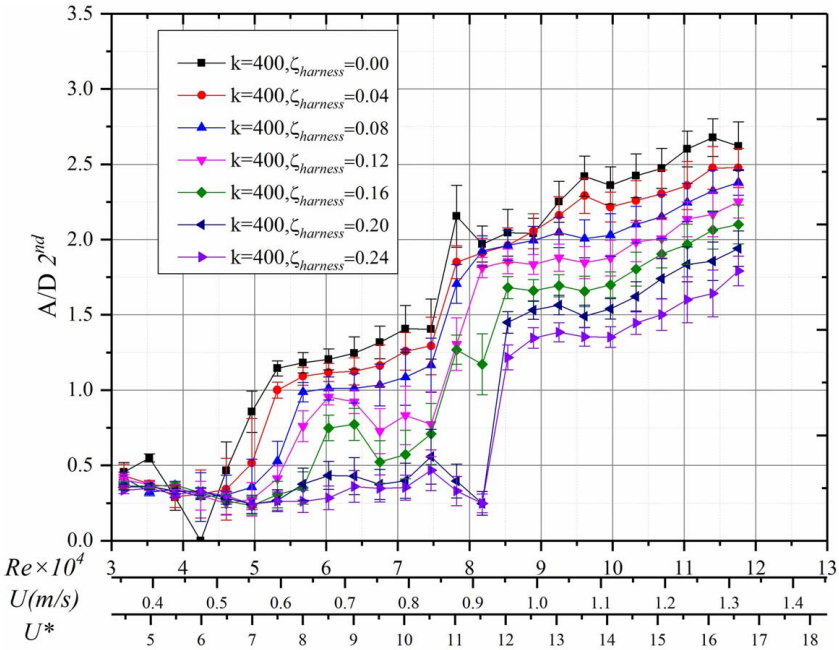

Fig. 13 Amplitude ratio *A/D* of the second cylinder for $K = 400$ N/m and $L/D = 2.57$

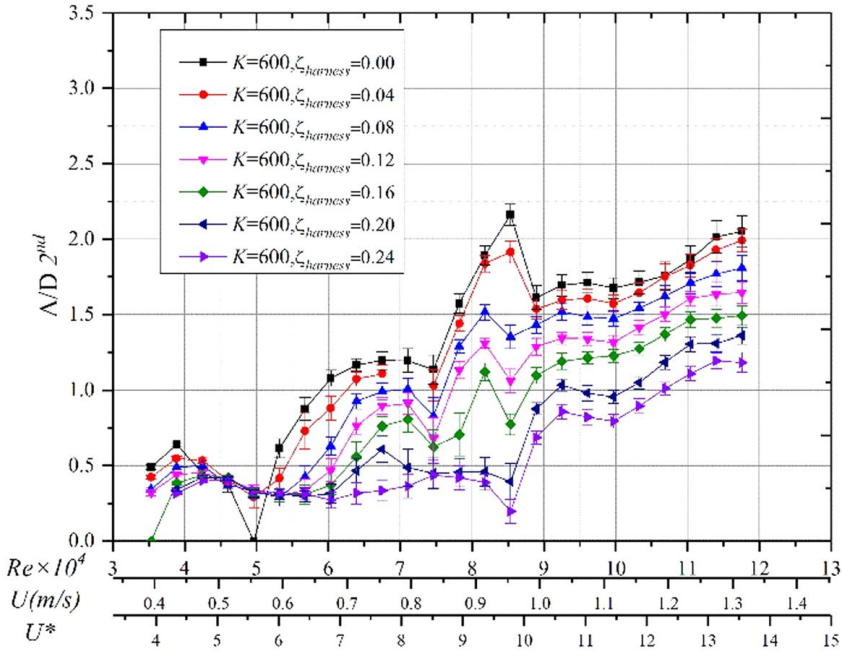

Fig. 14 Amplitude ratio *A/D* of the second cylinder for $K = 600$ N/m and $L/D = 2.57$

higher harnessing ratio ($\zeta harness > 0.12$), the oscillation either ceases or reduces significantly. Figures 21 and 22 shows that both the frequency and the oscillation speed are lower for the isolated cylinder.

(3) In the galloping region, the enhancement of the FIO for the first cylinder in tandem compared to the isolated cylinder is more pronounced than in other regions. Specifically, at the onset of galloping, the upstream cylinder reaches a high and stable oscillation earlier than the single cylinder. The *A/D* of the upstream cylinder is 23% higher while the frequency is the same for both cases, resulting in a higher power just for the upstream cylinder alone.

Case Study 1. In this case, only the $K = 400$ N/m results are presented. The rest of the spring-stiffness values tested exhibits the same trends. As can be seen from the discussion and Figs. 21 and 22, the oscillation of the upstream cylinder is enhanced due to the presence of the second cylinder. In the VIV region, the flow-induced oscillation is driven by the vortex shedding from the cylinder that induces alternating pressure difference and coupling with the restoring force from the springs. The presence of the rear cylinder (especially at an appropriate position) affects the vortex shedding of the upstream cylinder and, subsequently, the force on the upstream cylinder. Thus, the oscillation of the upstream cylinder is enhanced. In the galloping region, the presence of the rear cylinder contributes to the instability which drives galloping,

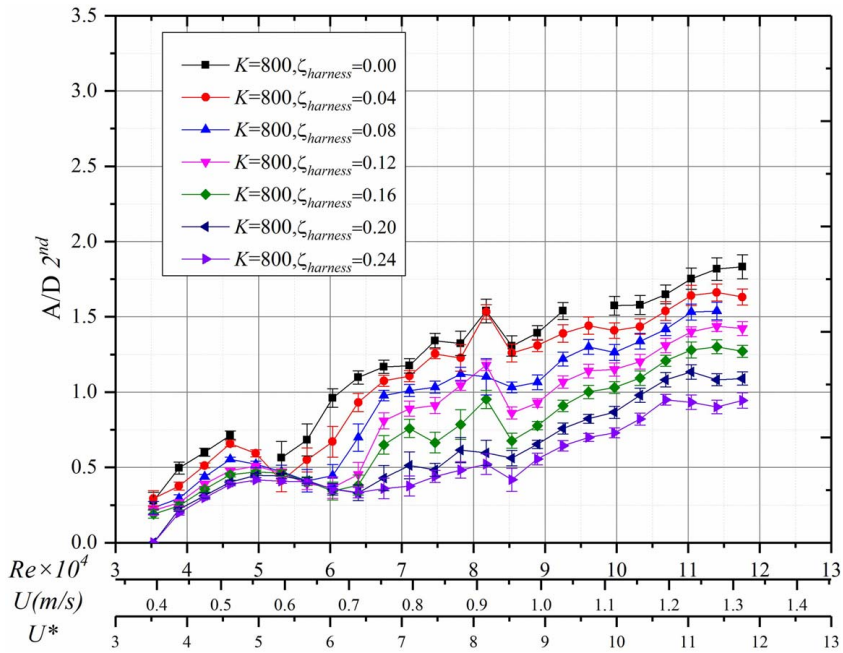

Fig. 15 Amplitude ratio *A/D* of the second cylinder for $K = 800$ N/m and $L/D = 2.57$

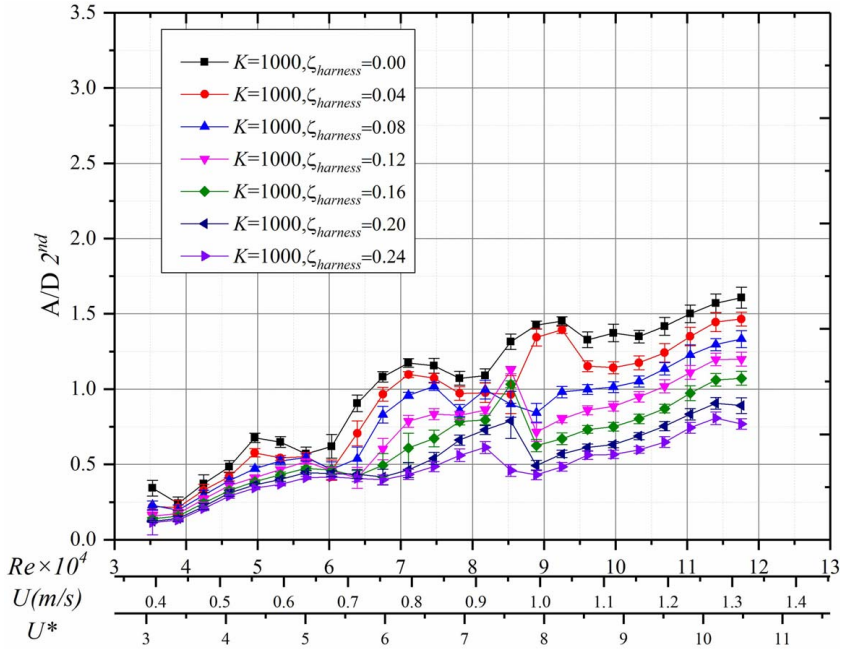

Fig. 16 Amplitude ratio *A/D* of the second cylinder for $K = 1000$ N/m and $L/D = 2.57$

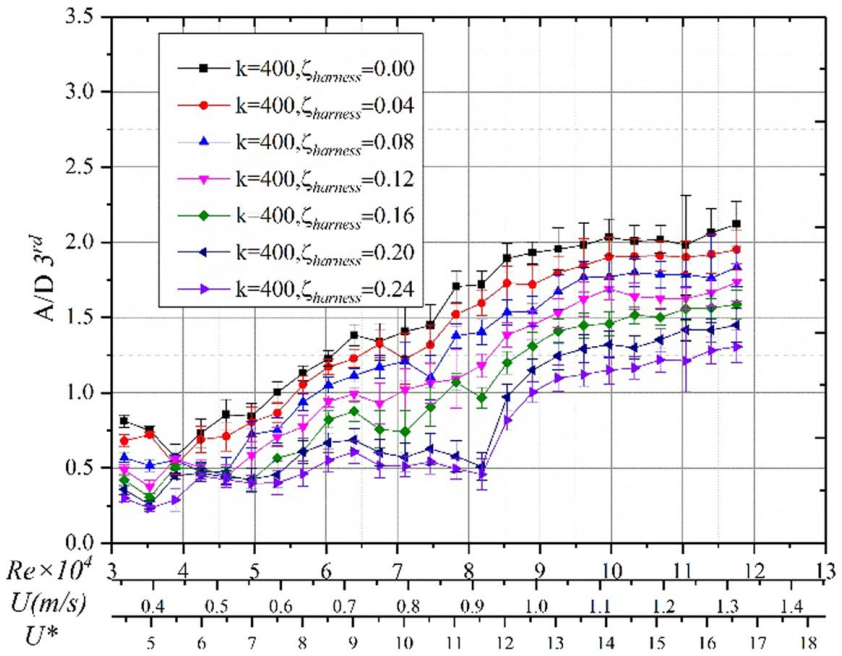

Fig. 17 The *A/D* of $K = 400$ N/m of the third cylinder at $L/D = 2.57$

further amplifying the FIO in the high flow velocity regions. This leads to enhancement of the harnessed power of the upstream cylinder regardless of the damping ratio [9].

Flow-Induced Oscillation of the Second Cylinder

(1) In all tests, in the range of the initial to upper VIV branch, the oscillation of the second cylinder is partially suppressed regardless of the damping and stiffness values. A plausible explanation is that at the initial VIV branch, the driving vortex force is from the shedding of predominantly 2S and S + P (single and pair) vortices. In this early stage, the presence of the third cylinder, as well as the wake vortex structure from the upstream cylinder, both shield the second cylinder from the incoming flow and interfere with its own wake. As the flow velocity increases, the oscillation becomes stable for the lower damping ratios. At higher damping, like ζharness = 0.20 and 0.24, the oscillation shows signs of suppression at the lower stiffness values $K =$ 400 N/m and 600 N/m, where the *A/D* of the former, at higher harnessed damping ratio 0.24, drops to 31% of the lower damping ratio 0.04 at Re = 71,000.

(2) Figures 23 and 24 show the displacement, fast Fourier transform (FFT), and phase portrait of the three cylinders at the initial branch and the transition. In Fig. 23, at Re = 38,900, the oscillation of the second cylinder shows a strong suppression and also show a delay pattern [25]. Which is, the

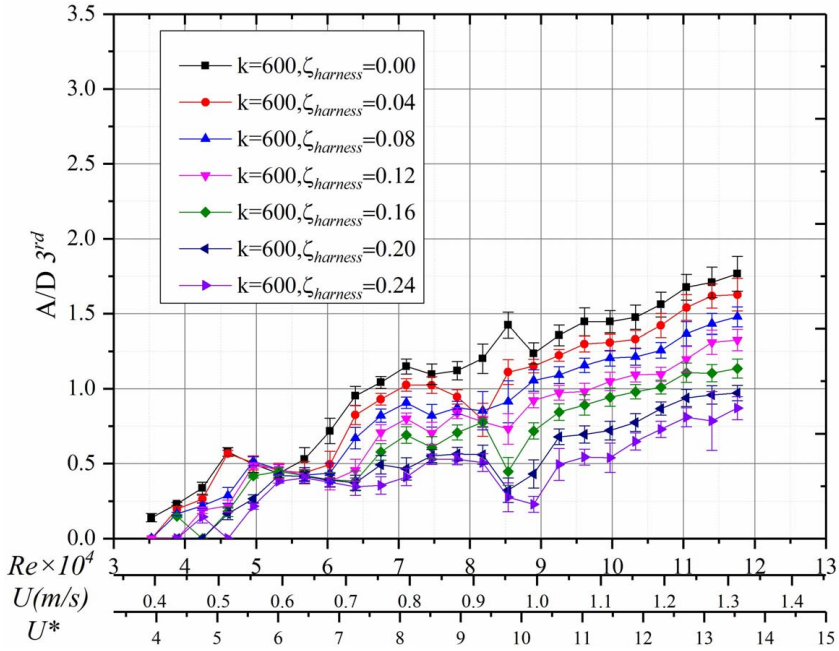

Fig. 18 The *A/D* of $K = 600$ N/m of the third cylinder at $L/D = 2.57$

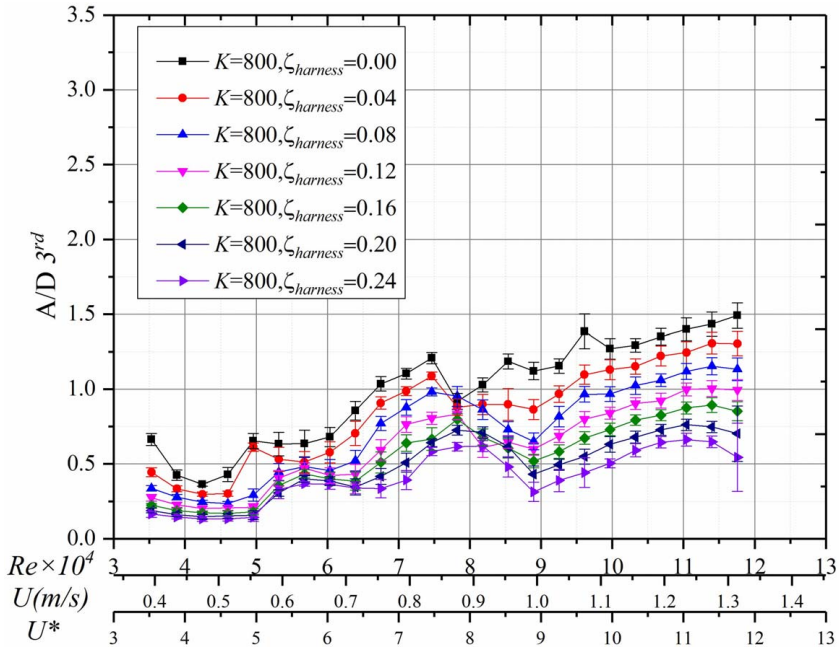

Fig. 19 The *A/D* of $K = 800$ N/m of the third cylinder at $L/D = 2.57$

oscillation frequencies are the same for three cylinders, and the second cylinder has 180 deg of difference than the first cylinder. In the typical transition of Fig. 24 at Re = 81,000, the oscillation of the third cylinder is suppressed, and all the cylinders oscillate in-phase at the same frequency.

Case study 2. Because of the position of the second cylinder, especially in the higher stiffness cases, there are almost no signs of the decrease in amplitude. For the lower damping ($\zeta_{harness} < 0.12$) of $K = 600$ and 800 N/m, the oscillation amplitude exceeds the upstream cylinder in the transition to the initial galloping region (around Re = 85,000). Expect the initial branch, the amplitude decrease as the damping increases for the second cylinders, and as the stiffness increases, the oscillation becomes stable as evidenced by the shorted error bars for higher stiffness cease.

(1) In the higher flow velocity, the FIO of the second cylinder becomes more stable than other flow regions. As shown in Figs. 12, 13, 21, and 22, the amplitude ratios increase as the flow velocity increases, albeit not as higher as the upstream cylinders (Fig. 5). The increase in amplitude, however, is not as sharp as for the single isolated cylinder.

Flow-Induced Oscillation of the Third Cylinder

(1) In the initial branch, the amplitude of the downstream cylinders at $K = 400$, 800, and 1000 N/m higher than the first and

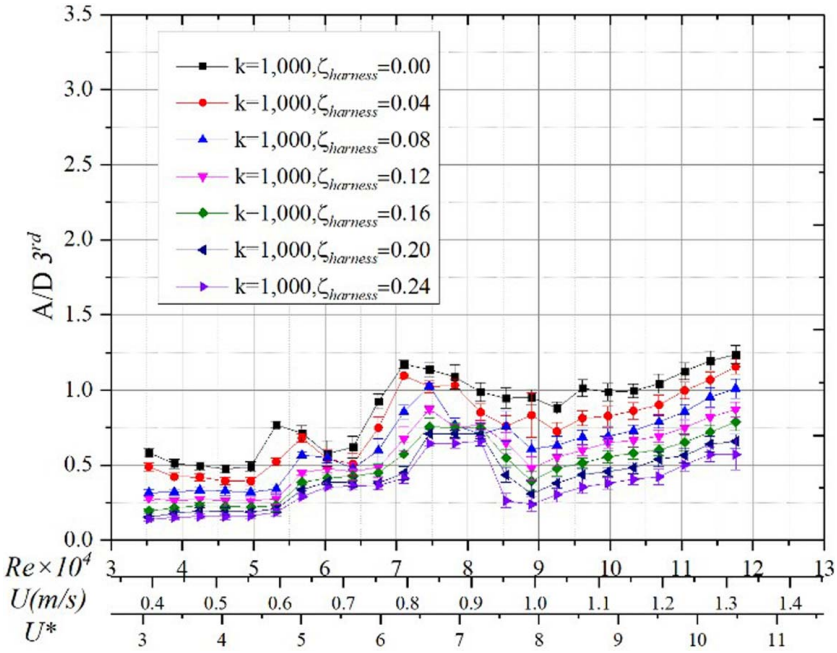

Fig. 20 The *A/D* of $K = 1000$ N/m of the third cylinder at $L/D = 2.57$

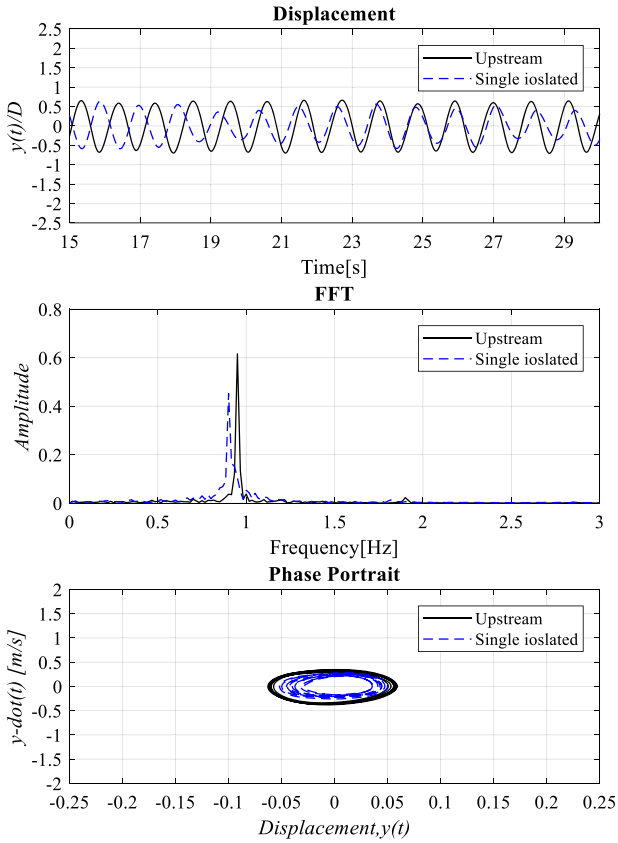

Fig. 21 Comparison of time history, frequency and phase portrait of the first cylinder in tandem and a single isolated cylinder at Re = 38,900 and $\zeta_{harness} = 0.16$

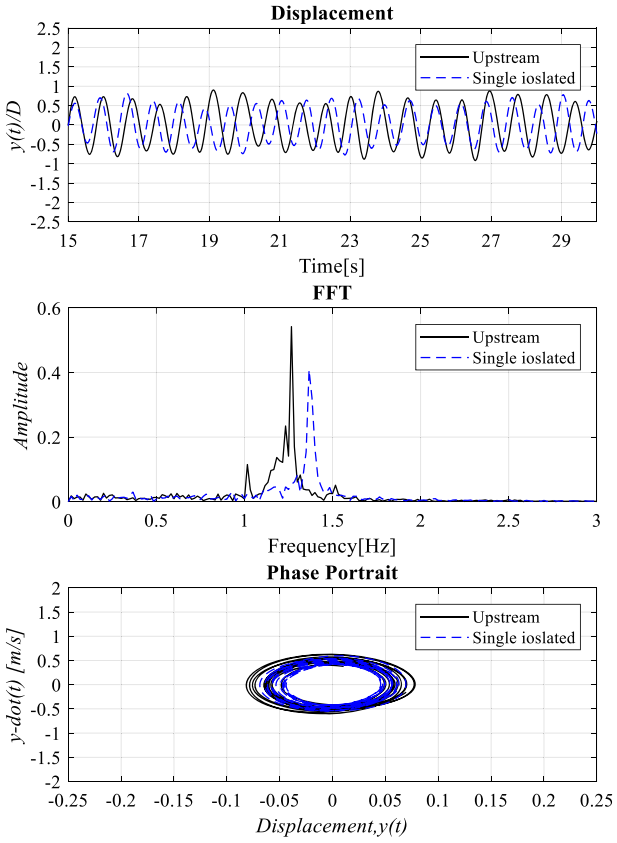

Fig. 22 Comparison of time history, frequency and phase portrait of the first cylinder in tandem and a single isolated cylinder at Re = 71,100 and $\zeta_{harness} = 0.12$

second cylinders, especially at lower harnessed damping ratios of 0.00 and 0.04. Because at the initial flow velocity of the VIV, since the vortexes are generated by the first two cylinders, even if the reduced velocity does not reach to the typical value, the alternating fluid force is enough for the initiation of VIV. Thus, the negative shielding effect [26] is not presented in most of the testing.

(2) For all the stiffness cylinders, the beginning of the upper branch is heavily suppressed. At this flow velocity, the typical vortex pattern is 2S (two single vortexes from every

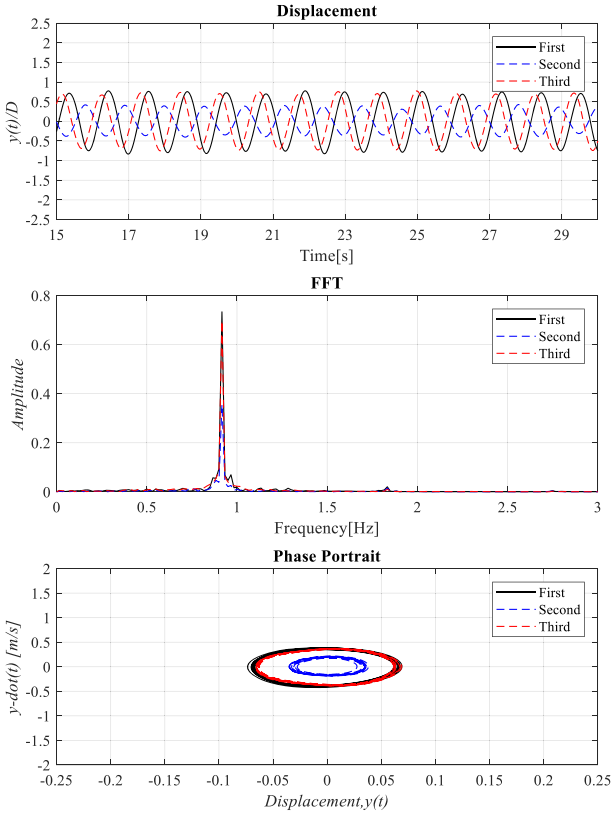

Fig. 23 Comparison of time history, frequency, and phase portrait of three cylinders at Re = 38,900 for $K = 400$ N/m and $\zeta_{harness} = 0.04$

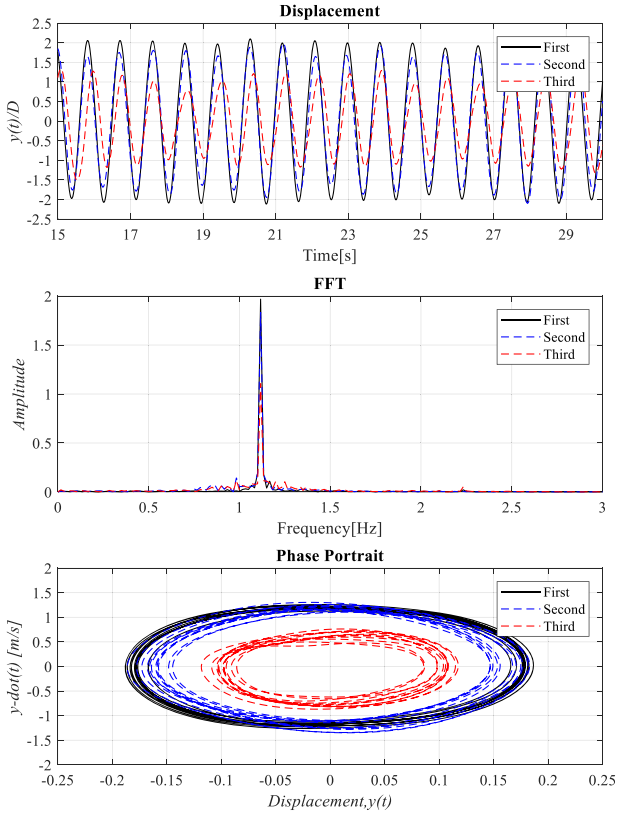

Fig. 24 Comparison of time history, frequency, and phase portrait of three cylinders at Re = 81,000 for $K = 600$ N/m and $\zeta_{harness} = 0.00$

cycle), since the shielding effect starts to impact the oscillation. Two factors contribute to such suppression of the third cylinder: the first is the aforementioned shielding, and the second reason is from the vortex disrupted by the presence of the upstream two cylinders, resulting in the 2S pattern now showing. Interestingly, as the flow increases, the amplitude (specifically for the lower ζharness) increases significantly compared to the middle cylinder, which, the downstream vortexes are disrupted by this cylinder despite the $L/D = 2.57$ spacing. The drops are also obvious as the damping ratio increases. For instance, as the damping ratio ζharness increases from 0.00 to 0.16, the amplitude decrease from 1.25 to 0.64 with a 50% drop.

(3) In the galloping region, there is a noticeable drop in the amplitude in the higher stiffness (natural frequency) cylinders. Particularly, in the highest stiffness $K = 1000$ N/m, the A/D, regardless of the damping ratios, is around 50% of the upstream cylinder. However, the standard deviation of the oscillation becomes much lower as the stiffness increases, indicating stable oscillation at a higher natural frequency. This is due to the vortex from the first and second cylinders

(4) Suppression of the amplitude ratios of the thirds cylinder, of all the stiffness, can be observed. Specifically, at the initial branch (Re < 40,000), the oscillation amplitude of the third exceeds the amplitude of the first and second cylinders. This can be seen as a result of the downstream of the cylinder that does not have the obstruction/present of another cylinder, which, combined with the vortexes from the upstream cylinders, enhances the FIO.

4.3 Harnessed Power Comparison. Figure 25 shows the test results for harnessed power for three tested additional damping ratios $\zeta_{harness} = 0.16$, 0.20, and 0.24. The figure is reproduced from Refs. [8,9]. The independent variable is the Reynolds number. To facilitate understanding the results, the absolute velocity and the reduced velocity, which are proportional to the flow velocity, are also presented parallel to the x-axis. Comparisons between the single isolated cylinder and multiple cylinders are listed in Tables 4–6.

Figure 25 shows the power harnessed by three tandem cylinders in comparison with a single isolated cylinder. The synergy of the cylinder/s and some important qualitative observations can be identified in two regions:

(a) $30{,}000 \le \text{Re} \le 85{,}000$: VIV and transition ranges.
- The harnessed power linearly increases as the flow velocity increases. Unlike the single-cylinder case, the power of multiple cylinders was initiated at lower Reynolds in the initial branch.
- Aside from the ceasing oscillation for a single cylinder, increasing the additional damping ratio does not increase the harnessed power by much in the cases tested, even though in VIV the amplitude decreases as the damping increases.
- In the lower branch, the harnessed power in the multiple cylinder cases does not drop like the single-cylinder case. The harnessed power is 3.3 times of the single isolated cylinder, and for three tandem cylinders, the number is 3.0 times of the single-cylinder case (Fig. 25(*a*)).
- Compared to the power of two tandem cylinders (Fig. 25), the power of three cylinders does not have an obvious drop in the lower branch, where the power of a single isolated cylinder drops significantly at higher $\zeta_{harness}$.

(b) $85{,}000 \le \text{Re}$ is the galloping region.
- In the initial galloping range, the synergistic FIO of multiple cylinders greatly enhances the harnessed power, as shown in Tables 4–6. Due to the geometry of the single

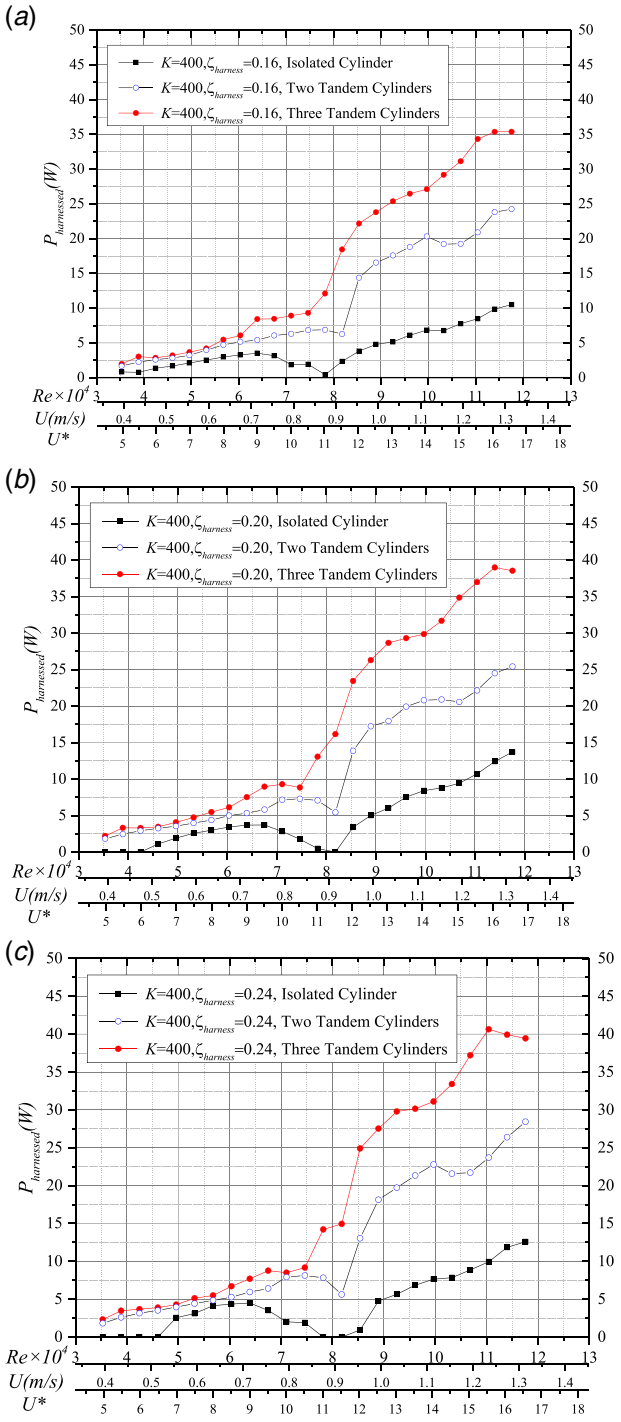

Fig. 25 Harnessed power of single isolated, two and three tandem cylinders at $K = 400$ N/m, $m^* = 1.343$, and $L/D = 2.01$: $\zeta_{harness} = 0.16$ (*a*), 0.20 (*b*), and 0.24 (*c*)

PTC cylinder, the turbulence stimulation (PTC) causes asymmetry which leads to galloping instability. The onset velocity of galloping is decided by the damping of the oscillator [8].

- In all the damping values tested, the power of three tandem cylinders is more than three times that of the single cylinder.
- At the last flow velocities tested, the power of three cylinders drops due to tip-flow and flow three-dimensionality effects. The amplitude of the third cylinder decreases.

Table 4 Comparison of tandem cylinders with an isolated cylinder for $\zeta_{harness} = 0.16$

U (m/s)	Harnessed power (W)			Ratio of two to a single isolated	Ratio of three to a single isolated
	Single	Two	Three		
0.95	3.83	14.36	22.17	3.77	5.82
1.03	5.14	17.58	25.36	3.42	4.93
1.15	6.76	20.31	29.18	3.00	4.31
1.19	7.75	19.20	31.13	2.48	4.01
1.23	8.47	19.24	34.32	2.27	4.05
1.27	9.85	20.89	35.36	2.12	3.59

Table 5 Comparison of tandem cylinders with an isolated cylinder for $\zeta_{harness} = 0.20$

U (m/s)	Harnessed power (W)			Ratio of two to an isolated	Ratio of three to an isolated
	Single	Two	Three		
0.95	3.40	13.86	23.43	4.07	6.88
1.03	6.03	17.94	28.66	2.97	4.74
1.15	8.79	20.71	31.68	2.36	3.60
1.19	9.42	20.88	34.86	2.22	3.70
1.23	10.73	20.55	36.96	1.91	3.44
1.27	12.41	22.13	38.99	1.78	3.14

Table 6 Comparison of tandem cylinders with an isolated cylinder for $\zeta_{harness} = 0.24$

U (m/s)	Harnessed power (W)			Ratio of two to an isolated	Ratio of three to an isolated
	Single	Two	Three		
0.95	0.94	13.04	24.91	13.85	26.46
1.03	5.65	19.73	29.79	3.49	5.26
1.15	7.84	22.79	33.41	2.90	4.26
1.19	8.86	21.58	37.22	2.43	4.19
1.23	9.95	21.70	40.65	2.18	4.08
1.27	11.85	23.70	39.93	1.99	3.36

5 Conclusions

The synergistic flow-induced oscillations and the hydrokinetic power conversion capacity of three rigid, circular tandem cylinders, with passive turbulence control, placed on end-springs, were investigated experimentally, for various values of harnessing damping for Reynolds numbers ($30{,}000 < \mathrm{Re} < 120{,}000$) at $K = 400$ N/m and center-to-center spacing of 2.01 diameters. Re range falls in the TrSL3, high-lift, flow regime. The following conclusions can be drawn:

(1) In the galloping range, the harnessed power by the three-cylinder converter shows a beneficial synergy between the three cylinders. The power harnessed by the three tandem cylinders is more than three times the corresponding single-cylinder power for the same parameters. For the tested value of cylinder spacing, three cylinders harnessed power between 3.36 and 5.82 times the power of a single cylinder.
(2) In the VIV range, the improvement due to the presence of the second and third cylinders is minimal and not worth the cost of designing a more complex converter.
(3) On the contrary, both in the transition from VIV to galloping and galloping, the power increase due to the synergy between three cylinders is multiple times the power generated by one cylinder under the same conditions, because in the transition the single isolated cylinder has little motion in this region.
(4) Regardless of the number of the cylinders, single or multiple in tandem, the oscillation frequencies in galloping remain equal to the $f_{n,water}$, albeit the amplitude variation of the downstream cylinders.

Based on this study, the future work on the multiple-cylinder VIVACE converter should be focused in two directions: (a) enhancing energy output of the downstream cylinders. Due to the shielding effect from the upstream cylinder, the downstream cylinders—especially the middle one—do not perform as well. (b) Introducing nonlinear oscillators in the tandem cylinders. Our studies found that the equivalent velocity of the downstream cylinders is lower because of the presence of the upstream cylinder. Thus, the optimal parameters of the cylinders are possibly not identical. So, nonlinear oscillators may have potential benefits because they adjust the parameters during FIO, which can yield potential benefits. Specifically, oscillators with nonlinear stiffness models [8,9], nonlinear damping models [27–29], and adaptive damping models [26] have been studied and tested in the MRELab.

Acknowledgment

This research was funded by the National Nature Science Foundation of China (Grant No. 51609053), the Natural Science Foundation of Heilongjiang Province (Grant No. YQ2019E017), and the Cooperative Agreement No. DE-EE0006780 between Vortex Hydro Energy, Inc. and the U.S. Department of Energy. The MRELab of the University of Michigan is a subcontractor through Vortex Hydro Energy. The research was also supported by the National Key Research and Development of China (Grant No. YS2017YFGH000163).

Conflict of Interest

There are no conflicts of interest.

Data Availability Statement

The data sets generated and supporting the findings of this article are obtainable from the corresponding author upon reasonable request. The authors attest that all data for this study are included in the paper. Data provided by a third party are listed in Acknowledgement.

References

[1] Bernitsas, M. M., and Raghavan, K., 2009, "Converter of Current, Tide, or Wave Energy," US Patent and Trademark Office, Patent No. 7,493,759 B2, Feb. 24.
[2] Bernitsas, M. M., and Raghavan, K., 2011, "Enhancement of Vortex Induced Forces & Motion Through Surface Roughness Control," US Patent and Trademark Office, Patent No. 8,047,232 B2, Nov. 1.
[3] Bernitsas, M. M., 2016, "Harvesting Energy by Flow Included Motions", *Chapter 47, Springer Handbook of Ocean Engineering*, M. R. Dhanak and N. I. Xiros, eds., Springer-Verlag, Berlin/Heidelberg.
[4] Lacey, R. W. J., Neary, V. S., Liao, J. C., Enders, E. C., and Tritico, H. M., 2011, "The Ipos Framework: Linking Fish Swimming Performance in Altered Flows From Laboratory Experiments to Rivers," River Res. Appl., **28**(4), pp. 429–443.
[5] Sun, H., Kim, E. S., Nowakowski, G., Mauer, E., and Bernitsas, M. M., 2016, "Effect of Mass-Ratio, Damping, and Stiffness on Optimal Hydrokinetic Energy Conversion of a Single, Rough Cylinder in Flow Induced Motions," Renewable Energy, **99**, pp. 936–959.
[6] Ding, L., Zhang, L., Kim, E. S., and Bernitsas, M. M., 2015, "URANS vs. Experiments of Flow Induced Motions of Multiple Circular Cylinders With Passive Turbulence Control," J. Fluids Struct., **54**, pp. 612–628.
[7] Kim, E. S., and Bernitsas, M. M., 2016, "Performance Prediction of Horizontal Hydrokinetic Energy Converter Using Multiple-Cylinder Synergy in Flow Induced Motion," Appl. Energy, **170**, pp. 92–100.
[8] Sun, H., Kim, E. S., Bernitsas, M. P., and Bernitsas, M. M., 2015, "Virtual Spring–Damping System for Flow-Induced Motion Experiments," ASME J. Offshore Mech. Arct. Eng., **137**(6), p. 061801.
[9] Sun, H., Ma, C., Kim, E. S., Nowakowski, G., Mauer, E., and Bernitsas, M. M., 2017, "Hydrokinetic Energy Conversion by Two Rough Tandem-Cylinders in Flow Induced Motions: Effect of Spacing and Stiffness," Renewable Energy, **107**, pp. 61–80.
[10] Zdravkovich, M. M., 1997, *Flow Around Circular Cylinders*, Vol. 1, E. Achenbach, ed., Oxford University Press, Oxford, UK.
[11] Zhang, L. B., Dai, H. L., Abdelkefi, A., and Wang, L., 2019, "Experimental Investigation of Aerodynamic Energy Harvester With Different Interference Cylinder Cross-Sections," Energy, **167**, pp. 970–981.
[12] Zhao, M., 2013, "Flow Induced Vibration of two Rigidly Coupled Circular Cylinders in Tandem and Side-by-Side Arrangements at a Low Reynolds Number of 150," Phys. Fluids, **25**(12), p. 123601.
[13] Zhao, M., Kaja, K., Xiang, Y., and Cheng, L., 2016, "Vortex-Induced Vibration of Four Cylinders in an In-Line Square Configuration," Phys. Fluids, **28**(2), p. 023602.
[14] Wolfgang, M. J., Anderson, J. M., Grosenbaugh, M. A., Yue, D. K., and Triantafyllou, M. S., 1999, "Near-Body Flow Dynamics in Swimming Fish," J. Exp. Biol., **202**(17), pp. 2303–2327.
[15] Han, Z., Zhou, D., He, T., Tu, J., Li, C., Kwok, K. C., and Fang, C., 2015, "Flow-Induced Vibrations of Four Circular Cylinders With Square Arrangement at Low Reynolds Numbers," Ocean Eng., **96**, pp. 21–33.
[16] Gao, Y., Yang, K., Zhang, B., Cheng, K., and Chen, X., 2019, "Numerical Investigation on Vortex-Induced Vibrations of Four Circular Cylinders in a Square Configuration," Ocean Eng., **175**, pp. 223–240.
[17] Park, H. R., Bernitsas, M. M., and Chang, C. C., 2013, "Robustness of the map of Passive Turbulence Control to Flow-Induced Motions for a Circular Cylinder at $30{,}000 < \mathrm{Re} < 120{,}000$," Proceedings of 31st OMAE 2013 Conference, Nantes, France, June.
[18] Park, H., Kumar, R. A., and Bernitsas, M. M., 2013, "Enhancement of Flow-Induced Motion of Rigid Circular Cylinder on Springs by Localized Surface Roughness at $3 \times 10^4 \leq \mathrm{Re} \leq 1.2 \times 10^5$," Ocean Eng., **72**, pp. 403–415.
[19] Lee, J. H., Xiros, N., and Bernitsas, M. M., 2011, ". "Virtual Damper–Spring System for VIV Experiments and Hydrokinetic Energy Conversion," Ocean Eng., **38**(5–6), pp. 732–747.
[20] Bernitsas, M. M., Ben-Simon, Y., Raghavan, K., and Garcia, E. M. H., 2009, "The VIVACE Converter: Model Tests at High Damping and Reynolds Number Around 105," ASME J. Offshore Mech. Arct. Eng., **131**(1), p. 011102.
[21] Blevins, R. D., 1990, *Flow-Induced Vibration*, 2nd ed., Van Nostrand Reinhold, New York.
[22] Foulhoux, L., and Bernitsas, M. M., 1993, "Forces and Moments on a Small Body Moving in a 3D Unsteady Flow (With Applications to Slender Structures)," ASME J. Offshore Mech. Arct. Eng., **115**(2), pp. 91–104.
[23] Morison, J. R., Johnson, J. W., and Schaaf, S. A., 1950, "The Force Exerted by Surface Waves on Piles," J. Pet. Technol., **2**(5), pp. 149–154.
[24] Bernitsas, M. M., Ofuegbe, J., Chen, J. U., and Sun, H., 2019, "Eigen-Solution for Flow Induced Oscillations (VIV and Galloping) Revealed at the Fluid-Structure Interface," ASME 2019 38th International Conference on Ocean, Offshore and Arctic Engineering, Glasgow, Scotland, UK, June 9–14.
[25] Sun, H., Ma, C., Kim, E. S., Nowakowski, G., Mauer, E., and Bernitsas, M. M., 2019, "Flow-Induced Vibration of Tandem Circular Cylinders With Selective Roughness: Effect of Spacing, Damping and Stiffness," Eur. J. Mech. B. Fluids, **74**, pp. 219–241.
[26] Sun, H., Bernitsas, M. M., and Turkol, M., 2020, "Adaptive Harnessing Damping in Hydrokinetic Energy Conversion by Two Rough Tandem-Cylinders Using Flow-Induced Vibrations," Renewable Energy, **149**, pp. 828–860.
[27] Ma, C., Sun, H., Nowakowski, G., Mauer, E., and Bernitsas, M. M., 2016, "Nonlinear Piecewise Restoring Force in Hydrokinetic Power Conversion Using Flow Induced Motions of Single Cylinder," Ocean Eng., **128**, pp. 1–12.
[28] Ma, C., Sun, H., and Bernitsas, M. M., 2018, "Nonlinear Piecewise Restoring Force in Hydrokinetic Power Conversion Using Flow-Induced Vibrations of Two Tandem Cylinders," ASME J. Offshore Mech. Arct. Eng., **140**(4), p. 041901.
[29] H. Sun, C. Ma, and M.M. Bernitsas, 2018. "Hydrokinetic Power Conversion Using Flow Induced Vibrations With Nonlinear (Adaptive Piecewise-Linear) Springs". Energy, **143**, pp. 1085–1106.